Single-layer planar on-chip flow cytometer using microfluidic drifting based three-dimensional (3D) hydrodynamic focusing†

Xiaole Mao,[ab] Sz-Chin Steven Lin,[a] Cheng Dong[b] and Tony Jun Huang*[ab]

Received 12th November 2008, Accepted 23rd February 2009
First published as an Advance Article on the web 12th March 2009
DOI: 10.1039/b820138b

In this work, we demonstrate an on-chip microfluidic flow cytometry system based on a three-dimensional (3D) hydrodynamic focusing technique, microfluidic drifting. By inducing Dean flow in a curved microfluidic channel, microfluidic drifting can be used to hydrodynamically focus cells or particles in the vertical direction and enables the 3D hydrodynamic focusing in a single-layer planar microfluidic device. Through theoretical calculation, numerical simulation, and experimental characterization, we found that the microfluidic drifting technique can be effectively applied to three-dimensionally focus microparticles with density and size equivalent to those of human CD4+ T lymphocytes. In addition, we developed a flow cytometry platform by integrating the 3D focusing device with a laser-induced fluorescence (LIF) detection system. The system was shown to provide effective high-throughput flow cytometry measurements at a rate of greater than 1700 cells s^{-1}.

Introduction

Flow cytometry is a powerful high-throughput, single-cell characterization tool that has a significant impact on both biomedical research and clinical diagnostics. In flow cytometry, the analysis is performed by passing a single-file cell stream through a focused laser beam at a rate of hundreds or even thousands of cells per second. Information regarding the size, type, and content of cells can be subsequently derived through the analysis of excited fluorescence emissions or scattered light arising from individual cells. For years, flow cytometry has been used in a wide variety of biomedical research fields such as immunology[1,2] and cancer biology.[3,4] In recent years, it has also become the method of choice for many clinical diagnostics. For example, CD4+ T lymphocyte flow cytometry counting is routinely conducted for diagnosing HIV.[5,6] However, the full potential of flow cytometry as a tool of research and clinical diagnostics has yet to be realized. Its high cost, mechanical complexity, bulky size, and need for highly trained personnel have limited its application.[7]

In order to make this technology more accessible to the public health care and biomedical research sectors, there have been great efforts in transforming flow cytometry systems to portable and mass-producible platforms.[8] In light of the nature of flow cytometry (interrogation of micron-scale cells or particles in tiny fluidic volumes), microfluidics appears to be a perfect solution to fulfil this mission. State-of-the-art microfluidic technology allows for the flexible and precise manipulation of microparticles in small integrated devices,[9] while cost-effective fabrication methods, such as soft-lithography,[10] enable mass-producible microfluidic devices.

One of the most important aspects of flow cytometry is to ensure the single-file passing of the cells through a focused laser beam so they can be interrogated one at a time. In conventional flow cytometry, this can be achieved by focusing the cell solution at the centre of the flow tube with the surrounding sheath flow using a co-axial injection flow chamber. Such flow chambers are difficult and expensive to manufacture using traditional bulk machining techniques. In microfluidic systems, alternative focusing schemes such as two-dimensional (2D)[11–13] or three-dimensional (3D)[14–22] hydrodynamic focusing are often implemented.

2D hydrodynamic focusing involves compressing the centre cell solution using horizontal (parallel to the device plane) sheath flows. One may readily fabricate the device for 2D hydrodynamic focusing using a standard soft-lithography technique; however, the lack of vertical focusing (normal to the device plane) may result in two or more cells simultaneously entering the detection region. The spreading of cells in the vertical direction was found to cause large measurement errors.[21,22] Further, the velocity variation of cells due to the flow velocity profile in the vertical direction could also result in variable signal integration time[23] and synchronization difficulties for down-stream cell sorting.[8]

3D hydrodynamic focusing is equivalently effective to co-axial focusing as it is capable of focusing cells in the centre of a channel using sheath flows from both horizontal and vertical directions; however, most 3D hydrodynamic focusing techniques developed so far rely on multi-layer 3D structures, which are not compatible with standard soft-lithography. The complex multi-step photolithography or multi-layer assembly protocols for these 3D structures compromise the advantages of microfluidics, making it difficult to develop mass-producible microfluidic flow cytometry systems. These problems call for a 3D hydrodynamic cell focusing technique, which is compatible with the standard soft-lithography and is capable of confining cells in both horizontal and vertical directions.

Recently, our group introduced a 3D hydrodynamic focusing technique named microfluidic drifting.[24] Compared to previously reported 3D hydrodynamic focusing methods, the uniqueness of

[a]*Department of Engineering Science and Mechanics, The Pennsylvania State University, University Park, PA 16802, USA. E-mail: junhuang@psu.edu; Fax: +1-814-865-9974; Tel: +1-814-863-4209*
[b]*Department of Bioengineering, The Pennsylvania State University, University Park, PA 16802, USA*

† Electronic supplementary information (ESI) available: Real-time video of Fig. 3c and Fig. 3d. See DOI: 10.1039/b820138b

this technique lies in its ability to achieve 3D hydrodynamic focusing in a single-layer planar (2D) microfluidic structure. As a result, the device can be readily fabricated *via* standard soft-lithography involving only one device layer and one photolithography mask, which makes it ideal for mass-producible flow cytometry devices.

In our previous publication, we demonstrated the concept of microfluidic drifting by the 3D hydrodynamic focusing of a fluorescent dye solution.[24] In this work, we aim to extend this technique for 3D cell focusing and practical high-throughput flow cytometry applications. When dealing with large microparticles, such as biological cells (on a length scale of several to several tens of microns), in practical flow cytometry measurements, microfluidic drifting based 3D hydrodynamic focusing becomes more challenging. These large microparticles, unlike small dye molecules ($\ll$ 1 μm), do not necessarily follow fluid streamlines due to prominent inertial effects[25–27] in high flow velocity regimes (on the order of m s^{-1})[16] often seen in high-throughput flow cytometry measurements. These effects may cause significant deviation of cell trajectory from the fluid streamlines in the microfluidic drifting process and render this technique inapplicable for practical flow cytometry measurements.

In this work, through combined theoretical, numerical and experimental studies, we demonstrate that our technique can be effectively applied to three-dimensionally focus microparticles with size and density equivalent to those of human CD4+ T lymphocytes, a type of cell which is routinely screened using flow cytometry assays for blood-related diseases. A home-made flow cytometry platform was developed by integrating the 3D focusing device with a laser-induced fluorescence (LIF) detection system. We show that the system is capable of providing effective high-throughput flow cytometry measurements.

Experimental

Design principle

The schematic of the 3D hydrodynamic focusing device and the principle of the microfluidic drifting based 3D hydrodynamic particle focusing is shown in Fig. 1. The device has four inlets, including one for cells or particles (A), one for the vertical focusing sheath flow (B), and two for horizontal focusing sheath flows (C and D). The device is 75 μm high throughout. The main channel is 100 μm wide and 1 cm long, and the radius of the curve (average of inner and outer portion) is 250 μm.

The 3D hydrodynamic particle focusing is a two-step process. The key to eliminating the need of a multi-layer 3D fluidic structure for focusing in the vertical direction is to utilize the Dean vortex[25–31] induced in a 2D curved channel. In the first step (insets 1–3), the particle flow and vertical focusing sheath flows were injected side-by-side from inlet A and B, respectively. The two flows converge and subsequently enter the 90° curve. In the curve, the induced Dean flow (inset 2), characterized by double-ring vortices in the cross-sectional plane, transversely accelerates the particles, sweeping the particles from the top and bottom of the channel toward the channel centre plane and further dragging them toward the opposite side of the channel. This step is termed

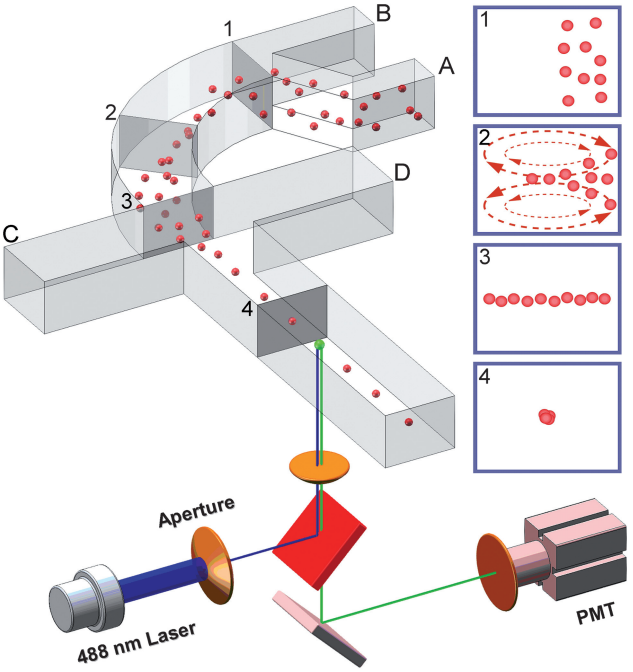

Fig. 1 Schematic of the device setup and microfluidic drifting mechanism. Inlet A: cells or particles; inlet B: vertical focusing sheath flow; Inlets C and D: horizontal focusing sheath flows. Insets (1–4) on the right show the particle distribution in the cross-sectional planes 1–4 during the 3D hydrodynamic focusing process. Arrowed-dash lines in inset 2 represent the Dean vortices.

'microfluidic drifting' and effectively 'focuses' the flowing particles in the vertical direction (inset 3). The second step (insets 3–4) focuses the particle flow in the horizontal plane using the horizontal sheath flows from inlets C and D. The combined effect of vertical and horizontal focusing is a three-dimensionally focused particle stream in the centre of channel's cross-sectional plane (inset 4). The flow injection rates are the same as in our previous publication (51.9 μl ml^{-1} for inlet A, 337.5 μl ml^{-1} for inlet B, and 225.5 μl ml^{-1} for inlets C and D).[24]

Device fabrication

The device was fabricated from polydimethylsiloxane (PDMS) using the standard soft-lithography technique. The PDMS replica mould was made on a silicon wafer by Deep Reactive Ion Etching (DRIE, Alcatel), and the etch depth (75 μm) was confirmed using a profilometer (KLA-Tencor). After DRIE etching, the silicon wafer was silanized by exposure to the vapour of 1*H*,1*H*,2*H*,2*H*-perfluorooctyl-trichlorosilane (Sigma-Aldrich). This silanization step helps to reduce the peeling damage when removing the PDMS from the mould, yielding a smooth PDMS channel sidewall to minimize the adhesion of particles. Inlets and outlets were drilled after the PDMS was peeled from the mould and the channel was subsequently sealed onto a glass slide. Polyethylene tubes were then inserted into the inlets and outlets to connect the device to syringe pumps (KDS 210, KD Scientific). Epoxy was used to seal the tube connection to prevent leaking due to the high pressure.

Detection system

The setup of the laser-induced fluorescence (LIF) system is also schematically shown in Fig. 1. The microfluidic 3D focusing device was mounted on an inverted fluorescence microscope (TE 2000U, Nikon). The excitation light was generated from an Argon laser (488 nm, 100 mW, Innova 300, Coherent). The fluorescence lamp house of the microscope was removed to allow the introduction of the laser into its epi-fluorescence optical path. The laser beam was focused and precisely aligned with the 3D focused particle stream using a 40× microscope object (N.A. = 0.6). The diameter of the focused laser beam was adjusted with an optical aperture in the light path. The fluorescent emission of particles while travelling through the laser beam was collected by the same lens and detected by a photo multiplier tube (PMT, Hamamatsu H6780-20). The signal was recorded using a digital oscilloscope (Tektronix DPO400) at a sampling rate of 2.5 MHz. A CCD camera (Photometrics CoolSNAP HQ2) was used to characterize the pattern of the particle flow during the 3D particle focusing process. A sideview imaging technique[24,31–34] was used to characterize the particle distribution in the vertical direction.

Fluorescent particles

Fluorescent polystyrene microparticles were purchased from Bangs Laboratories. Two types of particles were used in this study: 7.32 μm polystyrene particles with uniform fluorescence intensity (Dragon Green, excitation wavelength = 480 nm, emission wavelength = 520 nm), and 8.32 μm Dragon Green intensity standards (polystyrene particles with different levels of fluorescence intensities). The former was used to characterize the particle flow pattern during the 3D particle focusing process, and the latter was used for flow cytometry measurements. The size and density ($\rho = 1.05 \times 10^3$ kg m^{-3}) of both types of particles are equivalent to those of human CD4+ T lymphocytes ($\rho \approx 1.07 \times 10^3$ kg m^{-3}, diameter ≈ 8.5 μm),[35,36] making them ideal candidates for evaluating our 3D focusing technique for practical flow cytometry applications. All beads were diluted in 0.01% surfactant (SDS) solution to the desired concentration. Diluted particles were ultrasonicated for 10 min prior to experiments to prevent aggregation.

Numerical simulation

Numerical simulation of the 3D particle focusing process was conducted using a finite-volume (FV) based multi-physics package, ESI-CFD (ESI-CFD, USA). The 'flow module' and 'spray module' were employed to simulate the motion of discrete particles in the 3D focusing process.[27] The 'flow module' solves the governing mass, momentum, and energy conservation in an incompressible fluid flow. The 'spray module' tracks the trajectory of suspended particles by solving the force acted on the particles (*i.e.*, drag, buoyancy). The particles were randomly released from a rectangular virtual source area near the particle flow inlet at a zero initial velocity. The differencing scheme for particle motion was first-order Upwind. The Conjugates Gradient and Squared plus Preconditioning (CGS + Pre) solver were used to calculate the velocity field, and the Algebraic Multi-Grid (AMG) solver was used to solve the pressure. The convergence criterion was set to be 10^{-6} and the simulation was kept running for about 200 time steps until the 3D focusing was established. The computational grid contains 141 000 cells in total. A grid-density independent study was performed to ensure the sufficient grid density.

Results and discussions

Theoretical and numerical analysis of 3D hydrodynamic particle focusing process

Suspended particles, while travelling through a curved microchannel in a high flow velocity regime (on the order of m s^{-1}) often seen in high-throughput flow cytometry measurements, are subject to prominent inertial effects other than viscous drag and net buoyant/gravitational force, including inertial life forces due to the 'wall effect' and the shear gradient, and net centrifugal force.[25–27] Fig. 2a describes the force analysis of particles in the cross-sectional plane of the curved channel. Forces acting on suspended particles include the Dean viscous drag (F_D) due to the rotational Dean flow. The direction of F_D is dependent on the position of the particles. F_D plays a major role in microfluidic drifting by accelerating particles transversely to the main flow direction to first sweep the particles to the centre plane and then to drag particles toward the opposite side of the channel. Other forces include the inertial lift force (F_I), which causes particles to migrate across streamlines toward channel wall centres.[25–27] Particles (*i.e.*, polystyrene particles and lymphocyte cells) with a density higher than the carrier fluid (water) also experience net gravitational force (F_G), which precipitates particles, and net centrifugal force (F_{cfg}), which pulls particles away from the centre of the curvature. Assuming F_D to be the Stoke drag, the above mentioned forces can be estimated as:

$$F_D \sim 3\pi\mu U_D d \quad (1)$$

$$F_G \sim \tfrac{1}{6}(\rho_P - \rho_L) g \pi d^3 \quad (2)$$

$$F_{cfg} \sim \tfrac{1}{6}(\rho_P - \rho_L)\pi d^3 U_p^2 / R \quad (3)$$

and the ratio between F_I and F_D is:[37]

$$\frac{F_I}{F_D} \sim \frac{1}{\delta}\left(\frac{d}{D_h}\right)^3 Re^n \quad (n < 0) \quad (4)$$

Here, μ is the viscosity of the carrier fluid, U_D is the average Dean flow velocity which can be estimated using the CFD simulation, d is the diameter of particles, ρ_P and ρ_L are the densities of particles and the carrier fluid, U_p is the particle velocity, R is the radius of curvature of the curved channel, D_h is the hydraulic diameter defined as $2wh/(w + h)$ (w and h being the width and height of the channel), δ is the curvature ratio (D_h/R), and Re is the Reynolds number defined as $\rho_L U_L D_h/\mu$ (U_L being the average flow velocity).

When focusing small particles (for example, the fluorescent dye molecules in our previous publication[24]), F_D dominates the behaviour of particles because F_G, F_{cfg}, and F_I are negligible due to the small particle diameter (d). Therefore, these small particles are expected to travel along streamlines after being transversely accelerated by Dean vortices and be focused in the vertical

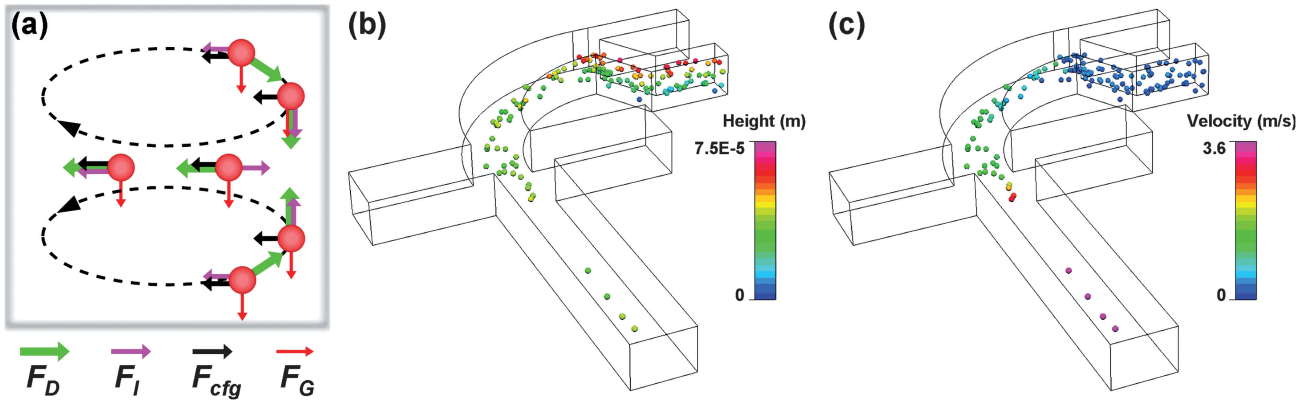

Fig. 2 (a) Force analysis diagram of particles in cross-sectional plane of the curved channel. Arrowed-dash lines represent the Dean vortices. (b) and (c) CFD simulation of 3D particle focusing processes. The simulations clearly indicate the particle 'drifting' phenomena in the curved channel and the final 3D focused single-file particle stream. Colour bars represent the particle height and velocity magnitude in (b) and (c), respectively.

direction during the microfluidic drifting process; however, F_D increases with the first power of the particle size while F_{cfg}, F_G, and F_I/F_D increase much faster with the third power, suggesting that particle size has a dramatic influence on F_{cfg}, F_G, and F_I. As a result, for much larger microparticles, such as biological cells with densities higher than those of the carrier fluid, F_{cfg}, F_G, and F_I may become dominant over F_D and compromise the 3D focusing by causing significant deviation of the particle trajectories in the microfluidic drifting process. Therefore, it is imperative to compare the relative magnitudes of these forces to assess the applicability of our microfluidic drifting technique in practical flow cytometry applications. Below are the parameters used in our calculation: particle radius $d = 8$ μm, $\rho_P = 1.07 \times 10^3$ kg m^{-3}, $\rho_L = 1.00 \times 10^3$ kg m^{-3}, and $U_p = U_L = 0.86$ m s^{-1}, and $U_D = 0.2$ m s^{-1} (estimated from the CFD simulation). The calculations show that F_D is on the order of ~10 nN whereas F_{cfg} and F_G are on the order of ~ 0.1 nN and ~0.1 pN, respectively, and F_I is less than 0.5% of the F_D. The calculated results suggest that, under the current flow conditions, Dean viscous drag is a dominant factor in the 3D particle focusing process. Therefore, particles are expected to travel along the streamlines, which converge towards the centre plane of the channel due to the Dean flow, and become vertically focused. Further calculations confirm that Dean drag dominates over gravitational, centrifugal, and inertial lift forces for a large range of particle sizes. These results suggest that the focusing of a wide variety of cells with different sizes (*i.e.*, bacteria $d \approx 1$ μm, neutrophils $d \approx 10$ μm, cancer cells $d \approx 15$ μm) is possible. The results also suggest that the use of density matching solution,[16,17] a method often practised to eliminate the gravitational effect in microfluidic 3D hydrodynamic particle-focusing devices, is not necessary in our case.

The results from the force scaling analysis are further supported by the numerical simulation. In Fig. 2b and 2c, we show the simulated 3D particle-focusing process. In simulation, particles were randomly injected from the particle inlet. The diameter of the particle was 8 μm and the density of the particle was 1.07×10^3 kg m^{-3}, and the flow condition was the same as the experiment. In the simulated results, both particle 'drifting' phenomena in the curved channel and the final 3D focused single-file particle stream were clearly visualized. In Fig. 2b, the colour of each particle represents its height (vertical direction). When particles first entered the inlet, different particle colours were observed, indicating variable particle heights. The variable colours of particles gradually changed to the uniform green colour while they travelled through the curved channel, suggesting that particles are being gradually focused at the same height in the vertical direction. After the horizontal focusing, it was clearly visualized that particles were lined up in a single-file fashion in the centre of the main channel. Fig. 2c shows the velocity distribution of the particles in the same process, and the colour of each particle represents their velocity magnitude. After 3D focusing, the cells were found to travel at the same velocity of approximately 3.6 m s^{-1}.

Experimental characterization of 3D particle focusing

To characterize the 3D particle focusing process, we imaged the particle flows in both the horizontal plane (topview) and the vertical plane (sideview). The experimental conditions were the same as previously indicated so that visual evidence of 3D hydrodynamic focusing could be obtained. Fig. 3a is a topview fluorescent image of the particle flow over a long exposure time (100 ms). It shows that after entering the 90° curve, particles start to 'drift' away from the centre of the curvature and the width of the particle flow is increased. During this process the particle flow is compressed toward the channel middle plane and stretched in the horizontal direction. The maximum width of the particle flow occurs at the exit of the 90° curve, after which the flow is further focused in the horizontal plane by horizontal focusing sheath flows. The final width in the horizontal plane of the focused stream was approximately 14 μm. The flow pattern of particles matches with that of the fluorescent dye solution obtained in our previous work,[24] suggesting negligible effects of large particle size in the microfluidic drifting process. Fig. 3b depicts the bright-field image of the same process and shows individual suspended particles. The overall particle distribution matches well with the simulated results in Fig. 2b and 2c.

Direct evidence of particle focusing in the vertical direction is shown through a sideview technique (Fig. 3c and 3d). Fig. 3c shows that before the 3D focusing process, streaks of fluorescent particles travel at different heights in the channel. Fig. 3d is a sideview image after the 3D focusing is in effect, and it clearly

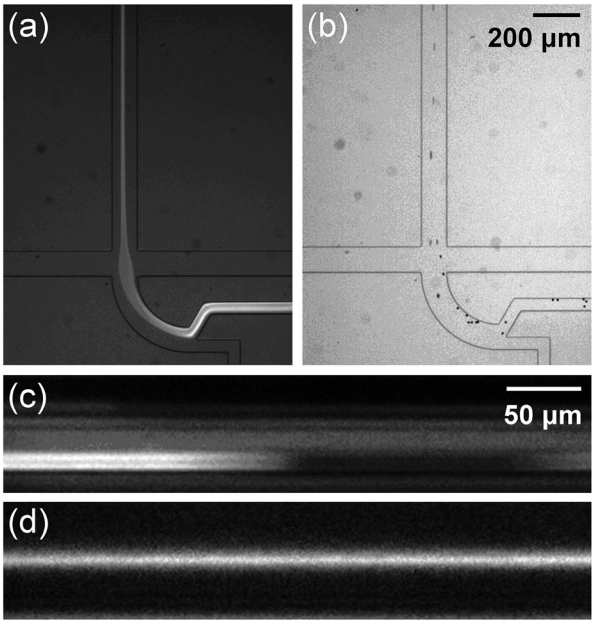

Fig. 3 (a) Fluorescent and (b) bright-field topview images of the particle flow pattern during the 3D hydrodynamic focusing process. Sideview images of the particle flow (c) before and (d) after the 3D particle focusing process.

shows the focusing of particles in the centre of the channel. The total height of the focused stream was estimated to be less than 12 μm. Therefore, we conclude that after the 'microfluidic drifting' based 3D hydrodynamic focusing process, particles are confined in a cross-sectional area of approximately 14 μm × 12 μm (less than twice the particle diameter in either direction). The 3D focusing process took less than 3 s to initialize (shown in a real-time video in the ESI†). We note that further optimization of flow focusing, such as reducing the height and width of the focused particle stream, is necessary to minimize the experimental error and to better suit the need for detection of smaller particles/cells. This can be achieved *via* modification of the flow parameters and geometry of the microfluidic channel. The cross-sectional area of the focused particle stream can be reduced by decreasing the ratio between the sample flow rate and total flow rate of all streams. Individual adjustment of the height or width of the focused particle stream is also possible. For example, reducing the flow rate ratio between the particle flow and the vertical focusing sheath flow may result in a smaller height throughout the focused stream; the width of the focusing particle stream can be reduced by increasing the horizontal focusing sheath flow rate. Changes of the channel geometries (*i.e.* angle or radius of the curved portion), as a subsequence of flow parameter changes, will also be necessary in order to achieve the optimized focusing result.

High-throughput flow cytometry measurements

For flow cytometry measurements, 3D particle focusing was first initialized and the focused particle stream was subsequently aligned with the laser beam. The size of the laser illumination region was estimated using a CCD camera. A circular laser beam, with a diameter of ~25 μm, was aligned with the particle stream to ensure the detection of all particles. The experiment was performed with a 1 : 1 mixture of two types of commercial flow cytometry intensity standards: 8.32 μm polystyrene particles with

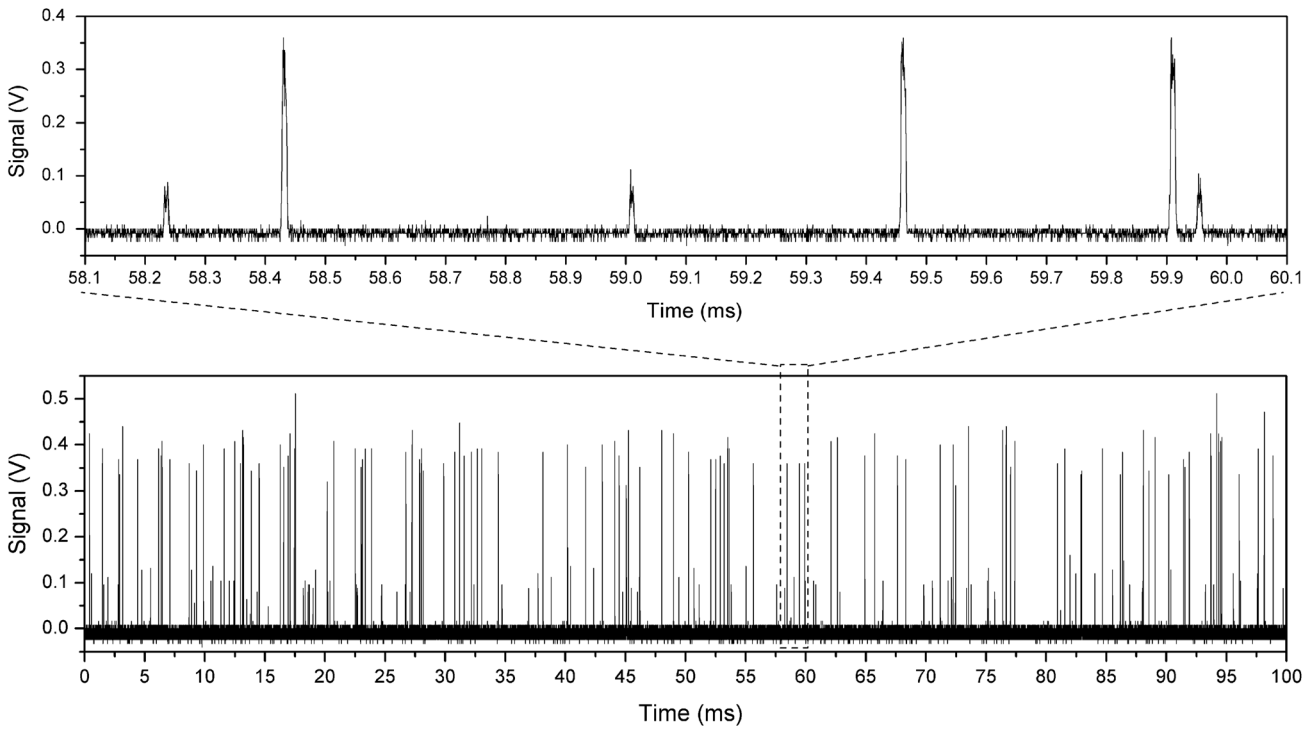

Fig. 4 A typical diagram of fluorescent peaks detected by the LIF system (100 ms recording time). Each peak represents the fluorescence emission of a single particle while passing through the laser illumination region. The upper inset is an amplified 2 ms interval.

nominal relative intensity being 21.9% for particle #1 and 100% for particle #2. The mixed particles were diluted in a 0.01% SDS solution to reach a final total concentration of $\sim 2 \times 10^6$ ml^{-1}. The particle solution was injected through the particle inlet A at a flow rate of 51.9 μl min^{-1}, which is equivalent to a particle flux of ~1730 particles s^{-1}. For each test, data were recorded for 4 s at a sampling rate of 2.5 MHz and analysed with a program written in Matlab. Fig. 4 shows a typical diagram of fluorescent peaks detected by the LIF system. Here, only a length of 100 ms is shown so that individual peaks can be identified. Two distinctive groups of peaks with their own characteristic heights are identified, each of which represents one type of fluorescent particle. An amplified view for a 2 ms interval was shown in the upper inset of Fig. 4. We observe that despite the height differences, all peaks show similar peak profiles.

The distribution of the peak heights for the entire 4 s data recorded is shown in Fig. 5. The characteristic peak height of each type of particle represents its fluorescent intensity. The histogram of the peak heights shows two well-separated, Gaussian-like distributions – one for each type of particle. The variation of the measured fluorescent intensity can be attributed to the inherent intensity variation of the particles and the measurement error due to the variation of particle vertical positions. The coefficients of variation (CV, standard deviation divided by the mean value) are 15.2% for particle #1 and 9.3% for particle #2, respectively. This result shows significant improvement over previously reported microfluidic flow cytometers (CV = 25–30%).[38–40] We attribute the low CV to the 3D hydrodynamic particle focusing, which minimizes the variation of particles' vertical positions while travelling through the optical detection region. The peak height distributions centre at ~0.099 and ~0.37 V, which correlate well with the nominal relative fluorescence intensities of two groups of particles (21.9% and 100%, respectively). The 4 s recorded data yielded a total count of 6965 peaks, which is equivalent to a peak frequency of 1741 particles s^{-1}. The peak count ratio is 49.0% (3410 peaks) for particle #1 and 51.0% (3555 peaks) for particle #2, respectively. Both the measured peak frequency and the peak count ratio match well with our experimental conditions. We also note in Fig. 4 that at the current experimental conditions fluorescent peaks are well separated, indicating a great potential to further improve the throughput of the system.

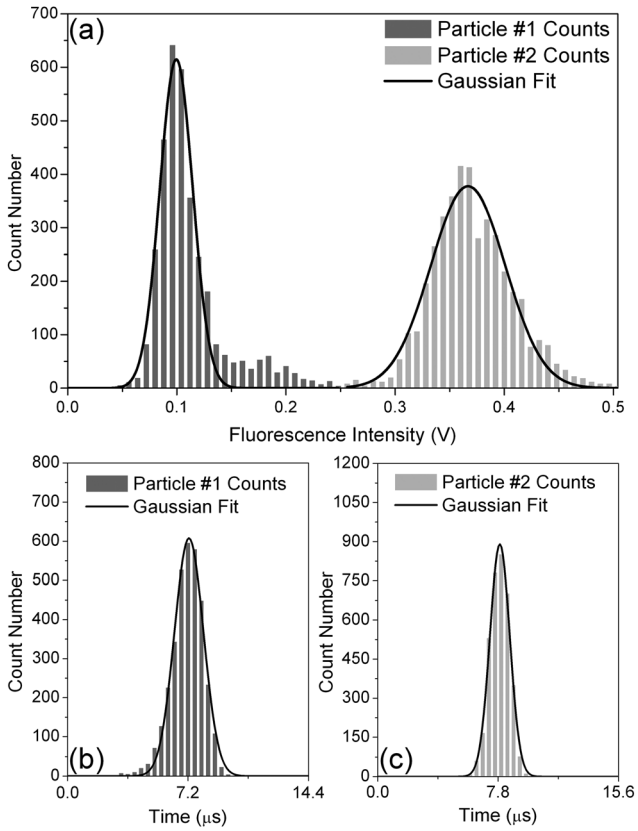

Fig. 5 (a) A histogram of the fluorescence peak height distribution. Two well-separated, Gaussian-like distributions are identified from the diagram representing two different types of particle. (b) and (c) Histograms of particle duration time through the detection area for particle #1 and #2, respectively. The difference between two distributions is statistically insignificant.

We further examined the distribution of the fluorescent peak width (Fig. 5b and 5c). The peak width represents the characteristic duration time of individual particles through the laser illumination region. In 2D hydrodynamic focusing, the particle velocity could vary across the entire range of the flow velocity profile – from virtually zero near the channel sidewalls to its maximum in the centre of the channel, resulting in a large duration time variation. In a 3D focused particle stream, such variation should be at a minimum as a result of all particles travelling at nearly the same velocity. Distributions of the full width at half maximum (FWHM) of peaks for particle #1 and #2 are shown in Fig. 5b and 5c. The difference between the two distributions is statistically insignificant. The mean duration times for the two particles are essentially the same: 7.2 μs for particle #1 and 7.8 μs for particle #2, respectively. The measured duration time is consistent with the particle velocity (~3.6 m s^{-1}) and laser beam size (~25 μm). The CV for the passage time distribution is only 11.9% for particle #1 and 8.1% for particle #2.

In this work only rigid polystyrene particles were tested. However, we do not expect problems in the future for the 3D focusing of real cells since studies have shown deformable cells to behave as rigid particles in straight and curving microchannels in a similar experimental setup.[25] The maximum flow velocity (~3.6 m s^{-1}) and minimum feature size (several tens of microns) of this study are also within the normal range of commercial flow cytometry devices.[16] Therefore, we do not anticipate the damage of the cells due to the high shear during the cell focusing either.

Conclusions

In summary, we have successfully demonstrated the potential of our microfluidic drifting based 3D hydrodynamic focusing technique in practical flow cytometry applications. Despite the large particle size and density mismatch, we show that our device can effectively focus microparticles equivalent to human CD4+ T lymphocytes in a high flow velocity regime, which are often encountered in flow cytometry measurements. Our calculation further confirms that this technique is potentially applicable for a wide variety of cells with different sizes, which is ideal for meeting highly diversified demands of flow cytometry applications.

The 3D focusing device was successfully integrated with a home-made LIF detection system, which demonstrated effective high-throughput flow cytometry measurements. The detection throughput is greater than 1700 particles s^{-1} and the device is potentially capable of even higher throughput. In addition, the device provides a low CV, which compares favourably among previously reported microfluidic flow cytometry devices.

The successful implementation of 3D hydrodynamic particle focusing and high-throughput flow cytometry measurements in a single-layer planar microfluidic device is an important step toward the miniaturization of entire flow cytometry systems. We believe that by integrating our device with the ongoing developments in soft-lithography-compatible in-plane optical components,[31,41–43] the microfluidic drifting technique can serve as an important basis for highly integrative, fully functional, and mass-producible microfluidic flow cytometry platforms.

Acknowledgements

Authors thank Dr Jeffrey D. Zahn and Dr Sung Yang for the help with the sideview imaging setup, Thomas R. Walker, Michael I. Lapsley, and Daniel Ahmed for helpful discussion, and Dr Jian Xu and Dr Chun-Feng Zhang for help with the instrumentation. This research was supported by National Science Foundation (ECCS-0824183 and ECCS-0801922) and the Penn State Centre for Nanoscale Science (MRSEC). Components of this work were conducted at the Penn State node of the NSF-funded National Nanotechnology Infrastructure Network (NNIN).

References

1 S. L. Liang, M. Slattery, D. Wagner, S. I. Simon and C. Dong, *Ann. Biomed. Eng.*, 2008, **36**, 661–671.
2 S. L. Liang, C. Fu, D. Wagner, H. Guo, D. Zhan, C. Dong and M. Long, *Am. J. Physiol.*, 2008, **294**, C743–C753.
3 J. You, A. M. Mastro and C. Dong, *Exp. Cell Res.*, 1999, **248**, 160–171.
4 C. Dong, M. J. Slattery, B. M. Rank and J. You, *Ann. Biomed. Eng.*, 2002, **30**, 344–355.
5 W. R. Rodriguez, N. Christodoulides, P. N. Floriano, S. Graham, S. Mohanty, M. Dixon, M. Hsiang, T. Peter, S. Zavahir and I. Thior, *PLoS Med.*, 2005, **2**, e182.
6 X. Cheng, D. Irimia, M. Dixon, K. Sekine, U. Demirci, L. Zamir, R. G. Tompkins, W. Rodriguez and M. Toner, *Lab Chip*, 2007, **7**, 170–178.
7 D. Huh, W. Gu, Y. Kamotani, J. B. Grotberg and S. Takayama, *Physiol. Meas.*, 2005, **26**, 73.
8 J. Gordin, C.-H. Chen, S. H. C. Cho, W. Qiao, F. Tsai and Y.-H. Lo, *J. Biophoton.*, 2008, **1**, 355–376.
9 J. Shi, X. Mao, D. Ahmed, A. Colletti and T. J. Huang, *Lab Chip*, 2008, **8**, 221–223.
10 Y. Xia and G. M. Whitesides, *Annu. Rev. Mater. Sci.*, 1998, **28**, 153–184.
11 N. Pamme, R. Koyama and A. Manz, *Lab Chip*, 2003, **3**, 187–192.
12 C. H. Lin and G. B. Lee, *J. Micromech. Microeng.*, 2003, **13**, 447–453.
13 P. Wong, Y. I. K. Lee and C. M. Ho, *J. Fluid Mech.*, 2003, **497**, 55–65.
14 R. Yang, D. L. Feeback and W. Wang, *Sens. Actuators, A*, 2005, **118**, 259–267.
15 C. Simonnet and A. Groisman, *Appl. Phys. Lett.*, 2005, **87**, 114104.
16 C. Simonnet and A. Groisman, *Anal. Chem.*, 2006, **78**, 5653–5663.
17 R. Scott, P. Sethu and C. K. Harnett, *Rev. Sci. Instrum.*, 2008, **79**, 046104.
18 N. Sundararajan, M. S. Pio, L. P. Lee and A. A. Berlin, *J. Microelectromech. Syst.*, 2004, **13**, 559–567.
19 C.-C. Chang, Z.-X. Huang and R.-J. Yang, *J. Micromech. Microeng.*, 2007, **17**, 1479–1486.
20 C.-H. Tsai, H.-H. Hou and L.-M. Fu, *Microfluid. Nanofluid.*, 2008, **5**, 827–836.
21 A. Wolff, I. R. Perch-Nielsen, U. D. Larsen, P. Friis, G. Goranovic, C. R. Poulsen, J. P. Kutter and P. Telleman, *Lab Chip*, 2003, **3**, 22–27.
22 S. Chung, S. J. Park, J. K. Kim, C. Chung, D. C. Han and J. K. Chang, *Microsyst. Technol.*, 2003, **9**, 525–533.
23 S. Eyal and S. R. Quake, *Electrophoresis*, 2002, **23**, 2653–2657.
24 X. Mao, J. R. Waldeisen and T. J. Huang, *Lab Chip*, 2007, **7**, 1260–1262.
25 D. Di Carlo, D. Irimia, R. G. Tompkins and M. Toner, *Proc. Natl. Acad. Sci. U. S. A.*, 2007, **104**, 18892.
26 D. DiCarlo, J. F. Edd, D. Irimia, R. G. Tompkins and M. Toner, *Anal. Chem.*, 2008, **80**, 2204–2211.
27 A. A. S. Bhagat, S. S. Kuntaegowdanahalli and I. Papautsky, *Lab Chip*, 2008, **8**, 1906–1914.
28 P. B. Howell, D. R. Mott, J. P. Golden and F. S. Ligler, *Lab Chip*, 2004, **4**, 663–669.
29 A. P. Sudarsan and V. M. Ugaz, *Lab Chip*, 2006, **6**, 74–82.
30 A. P. Sudarsan and V. M. Ugaz, *Proc. Natl. Acad. Sci. U. S. A.*, 2006, **103**, 7228–7233.
31 X. Mao, J. R. Waldeisen, B. K. Juluri and T. J. Huang, *Lab Chip*, 2007, **7**, 1303–1308.
32 J. Cao, S. Usami and C. Dong, *Ann. Biomed. Eng.*, 1997, **25**, 573–580.
33 J. Cao, B. Donell, D. R. Deaver, M. B. Lawrence and C. Dong, *Microvasc. Res.*, 1998, **55**, 124–137.
34 J. Leyton-Mange, S. Yang, M. H. Hoskins, R. F. Kunz, J. D. Zahn and C. Dong, *J. Biomech. Eng.*, 2006, **128**, 271.
35 T. J. Kipps and D. A. Carson, in *Williams hematology*, ed. E. Beutler, M. A. Lichtman, B. S. Coller, T. J. Kipps, U. Seligsohn and J. Prchal, McGraw-Hill, Columbus, 7th edn, 2005. ch. 75, p. 1031.
36 D. W. Inglis, J. A. Davis, T. J. Zieziulewicz, D. A. Lawrence, R. H. Austin and J. C. Sturm, *J. Immunol. Methods*, 2008, **329**, 151–156.
37 J. P. Matas, J. F. Morris and E. Guazzelli, *Oil. Gas Sci. Technol.*, 2004, **59**, 59–70.
38 Z. Wang, J. El-Ali, M. Engelund, T. Gotsæd, I. R. Perch-Nielsen, K. B. Mogensen, D. Snakenborg, J. P. Kutter and A. Wolff, *Lab Chip*, 2004, **4**, 372–377.
39 D. P. Schrum, C. T. Culbertson, S. C. Jacobson and J. M. Ramsey, *Anal. Chem.*, 1999, **71**, 4173–4177.
40 M. A. McClain, C. T. Culbertson, S. C. Jacobson and J. M. Ramsey, *Anal. Chem.*, 2001, **73**, 5334–5338.
41 J. Gordin, L. Victor and Y.-H. Lo, *Appl. Phys. Lett.*, 2006, **89**, 061106.
42 S. K. Y. Tang, C. A. Stan and G. M. Whitesides, *Lab Chip*, 2008, **8**, 395–401.
43 S. Camou, H. Fujita and T. Fujii, *Lab Chip*, 2003, **3**, 40–45.